Supplemental Information for "Single Photon Emission from Point Defects in Aluminum Nitride Films"

Yongzhou Xue,[1,§] Hui Wang,[2,§] Nan Xie,[2] Qian Yang,[1,3] Fujun Xu,[2] Bo Shen,[2] Jun-jie Shi,[2] Desheng Jiang,[1,3] Xiuming Dou,[1,3,*] Tongjun Yu,[2,*] and Bao-quan Sun[1,3,4,*]

[1]State Key Laboratory for Superlattices and Microstructures, Institute of Semiconductors, Chinese Academy of Sciences, Beijing 100083, China

[2]State Key Laboratory for Artificial Microstructures and Mesoscopic Physics, School of Physics, Peking University, Beijing 100871, China

[3]College of Materials Science and Optoelectronic Technology, University of Chinese Academy of Sciences, Beijing 100049, China

[4]Beijing Academy of Quantum Information Sciences, Beijing 100193, China

[§]Yongzhou Xue and Hui Wang contributed equally to the work.

[*]Address correspondence to xmdou04@semi.ac.cn, tongjun@pku.edu.cn, bqsun@semi.ac.cn

I. Experimental Apparatus

Figure S1 is a schematic of the home-built confocal microscope used in this work. A continuous wave 532 nm laser was used for the excitation in all spectral and $g^2(\tau)$ measurements. The laser beam was focused on the sample using a high numerical aperture objective (NA = 0.9). The emitted signal was collected by the same objective and spectrally filtered from the remaining pump light by a long-pass filter with wavelength cut-off at 550 nm, then analyzed using a 0.5 m monochromator equipped with a silicon charge-coupled device (CCD) for PL or two avalanche photodiodes (APD) for single photon counting measurements. Additionally, a HBT setup equipped with two silicon APDs was used to perform autocorrelation measurements, which were employed to verify the single-photon property. Cryogenic PL was done using a Montana Instruments cryostat equipped with an X-Y-Z nanocube system, and the temperature can be adjusted between 5 K and 350 K.

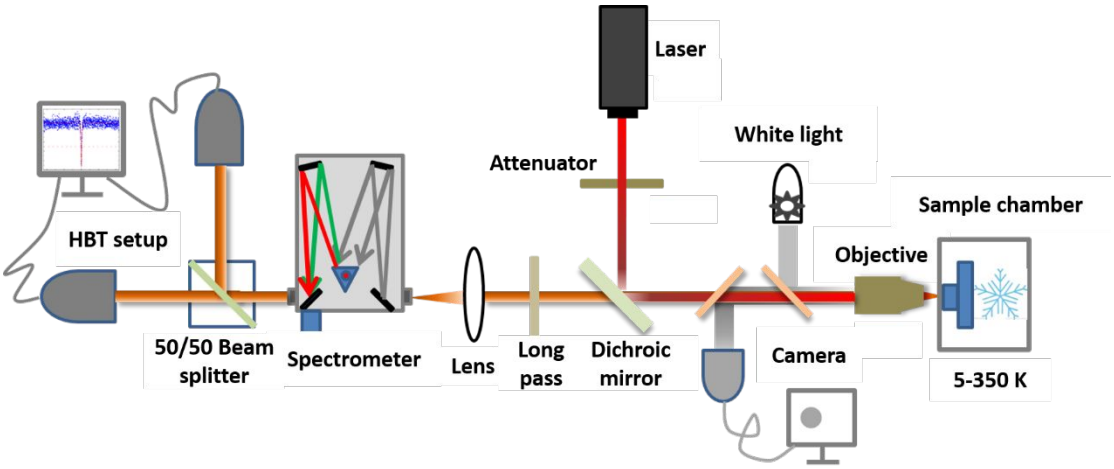

Figure S1. Schematic diagram of the optical confocal microscopy setup used in the experiment.

II. Second-order autocorrelation function $g^{(2)}(\tau)$ measurements

As shown in Fig. 2b in the main text, a histogram with a wavelength distribution of 74 SPEs is presented. Here, more measured PL spectra and $g^{(2)}(\tau)$ curves at 10 K from different point defects in AlN films are shown in Fig.S2. It can be seen that all the $g^{(2)}(0)$ values at a zero time delay are below the classical threshold of 0.5, which indicates that the emission is nonclassical and the emitters are SPEs.

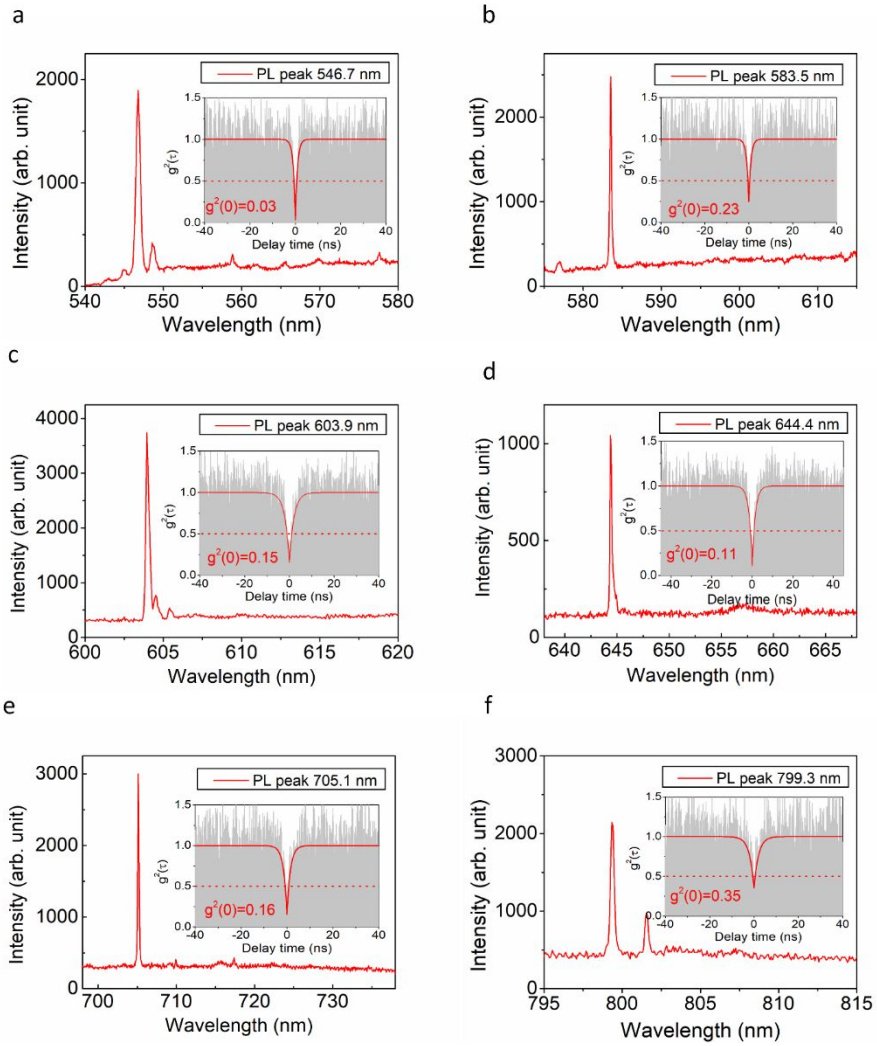

Figure S2. PL spectra for different point defects in AlN films. Inset: The corresponding $g^{(2)}(\tau)$ curves are presented, showing the emitters are SPEs, where the red dotted lines represent the classical threshold of 0.5.

Figure S3 shows the obtained $g^{(2)}(\tau=0)$ values as a function of wavelength for 74 defect emitters. It clearly demonstrates that all $g^{(2)}(\tau=0)$ values are less than 0.5, meaning that they are indeed SPEs.

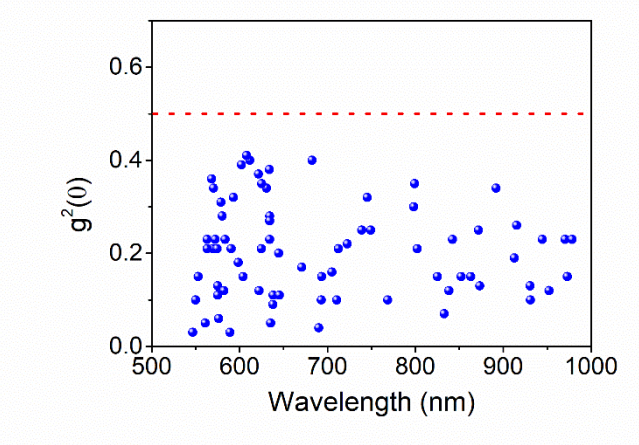

Figure S3. Measured $g^{(2)}(\tau=0)$ values as a function of wavelength for 74 emission lines in AlN. The classical threshold value of 0.5 is indicated by the dashed lines.

We also measured the second-order correlation function $g^{(2)}(\tau)$ for another two emitters over long delay times, as shown in Fig.S4(b) and (d), respectively. It shows a bunching effect at a longer time delay. Figures S4 (a) and (c) present the corresponding PL spectra with the emission wavelength of 580.38 nm and 690.24 nm at 10 K, with excitation laser power of 1 mW and 0.85 mW respectively. Here, the additional peak seen at 570 nm in Fig. S4 (a) is another defect peak, and the narrow peaks seen at around 692 nm in Fig. S4 (c) is the Cr impurity emission from the sapphire substrate. Figures S4 (b) and (d) show the second-order autocorrelation $g^{(2)}(\tau)$ measurements for correlation times of up to 2 μs, with the inset showing corresponding short-delay time $g^{(2)}(\tau)$ characteristics. Fitting the second-order autocorrelation measurements for the emitters with Eq. (1) (see main text) yield

$g^{(2)}(\tau = 0)$ values of 0.47 and 0.04, respectively. There are clear bunching behaviors of the SPEs, which means a long-lived metastable states exist in the single defect emitters of AlN.

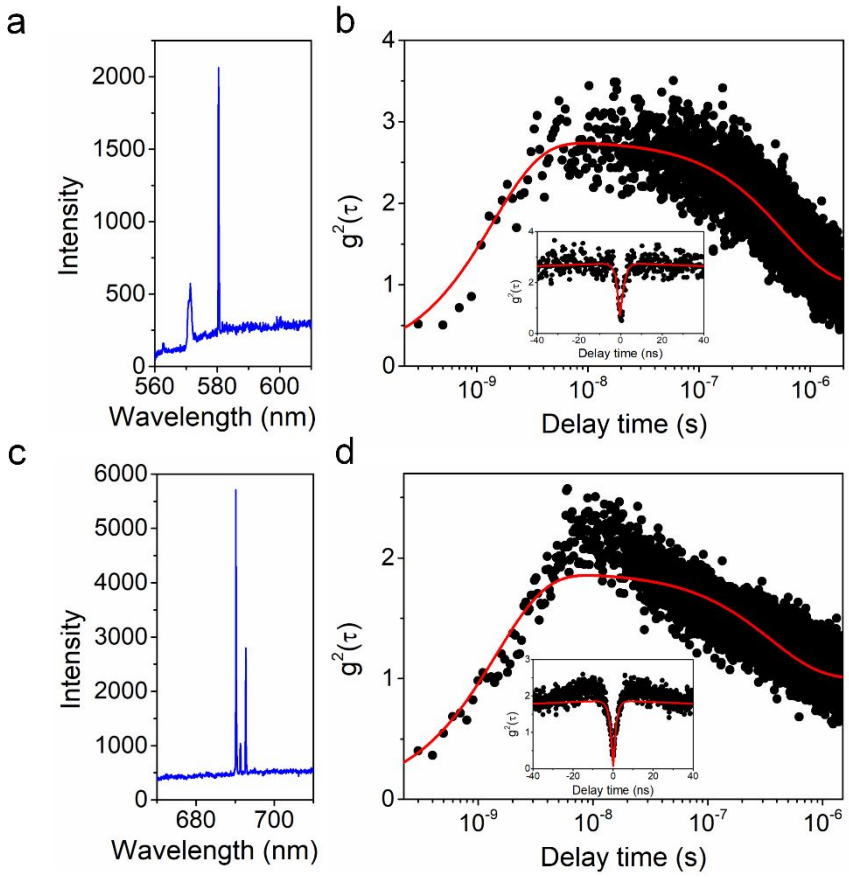

Figure S4. Low-temperature PL spectra and $g^{(2)}(\tau)$ measurements. (a) and (c) PL spectra with the emission wavelength of 580.38 nm and 690.24 nm respectively. (b) and (d) Second-order autocorrelation function $g^{(2)}(\tau)$ measurements over long delay times. Insets of (b) and (d) show the $g^{(2)}(\tau)$ curves of the same emitters at a short-time scale. The curves are fitted with three-level configuration with a long-lived metastable state, yielding the $g^{(2)}(\tau = 0)$ values of 0.47 and 0.04, respectively.

In addition, we have measured the second-order correlation functions $g^{(2)}(\tau)$ at longer delay time scales under different laser excitation powers. The PL spectrum

and $g^{(2)}(\tau)$ measurements are as shown below. Figure S5 (a) shows the saturated behavior of the PL intensity with increasing the excitation power, where the corresponding wavelength is 597.49 nm (see inset) at 10 K. The PL data here is corrected by subtracting the background and fitted by an expression of $I = I_{\infty}\frac{P}{P + P_{sat}}$, where P_{sat} is the saturated excitation power and I_{∞} corresponds to the saturated PL intensity. Fitting the background-corrected data yields a saturation power of 0.88 mW. Figure S5 (b)-(d) show the measured $g^{(2)}(\tau)$ curves under different laser powers of 0.26 mW, 0.85 mW and 1.8 mW, respectively. Fitting the $g^{(2)}(\tau)$ data by Eq. (1)(see main text) yields $g^{(2)}(\tau = 0)$ values of 0.34, 0.51, and 0.70, respectively. It demonstrates that the increase of $g^{(2)}(\tau = 0)$ values with excitation power is mainly due to the laser-induced background fluorescence. In general, some types of defects (V_N, V_{Al} and O_N, and their complex) may have relative larger population within AlN near threading dislocations which may induce background luminescence.[1,2]

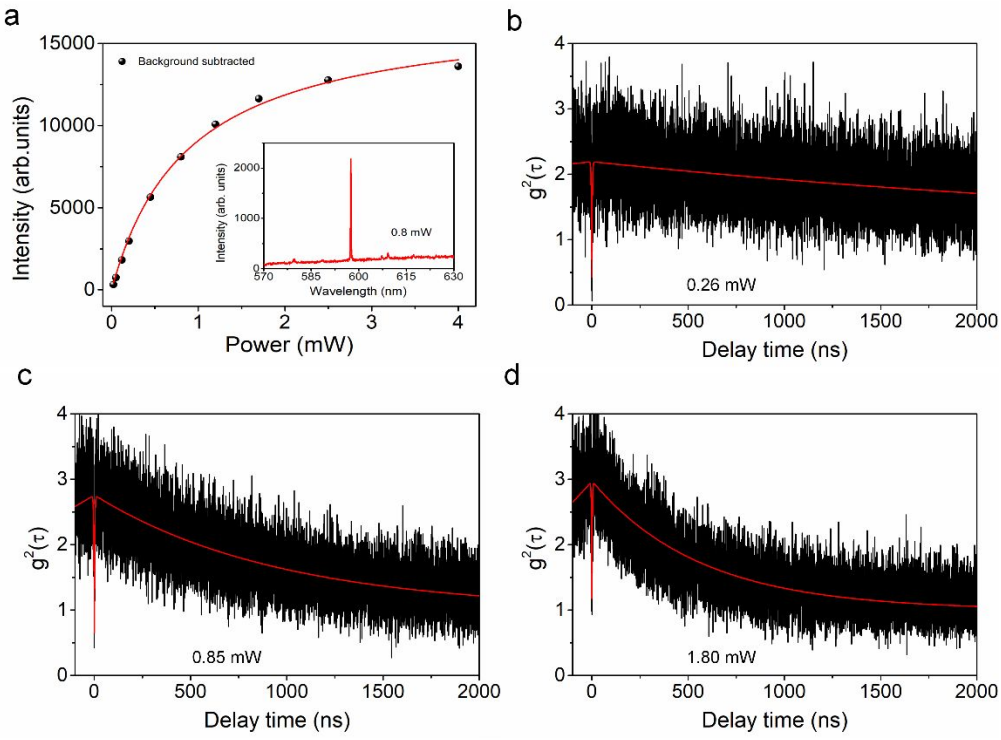

Figure S5. (a) PL intensity as a function of excitation power. The data here is corrected by subtracting the background fluorescence. The inset is the PL spectrum with the emission wavelength of 597.49 nm at the excitation power of 0.8 mW at 10 K. (b)-(d) The $g^{(2)}(\tau)$ characteristics measured under the excitation powers of 0.26, 0.85 and 1.80 mW, respectively and red curves are fitting results by using three-level model.

III. PL polarization profiles

The emitter's polarization property has been discussed in the main text, as shown in Fig.3d, which shows a high linear polarization for emission. Here, the visibility of the emission polarization for another 11 emitters are plotted in Fig.S6. It shows that the polarization visibility of emitters ranges from 78% to 99.9%.

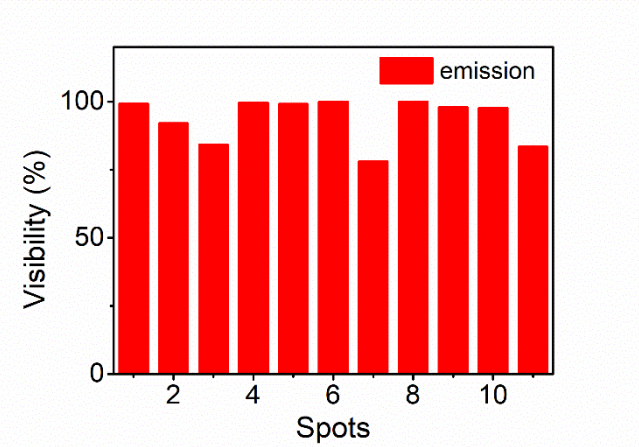

Figure S6. Polarization visibility of 11 emitters.

IV. Temperature-dependent FWHM

Two different types of temperature-dependent FWHM in AlN are presented in Fig.4 of the main text. Here, corresponding PL spectra as a function of temperature are presented in Fig. S7 (a) and (b). In addition, the temperature-dependent FWHMs of another 12 emitters have been measured. As described in the main text, a T^3 or

single exponential dependence can be used to describe the linewidth broadening as a function of temperature. Figure S7 (c) summarizes the statistical distribution of the two temperature-dependent FWHMs for 12 emitters, showing that there are 2 emitters having T^3 behavior and 10 emitters having single exponential behaviors.

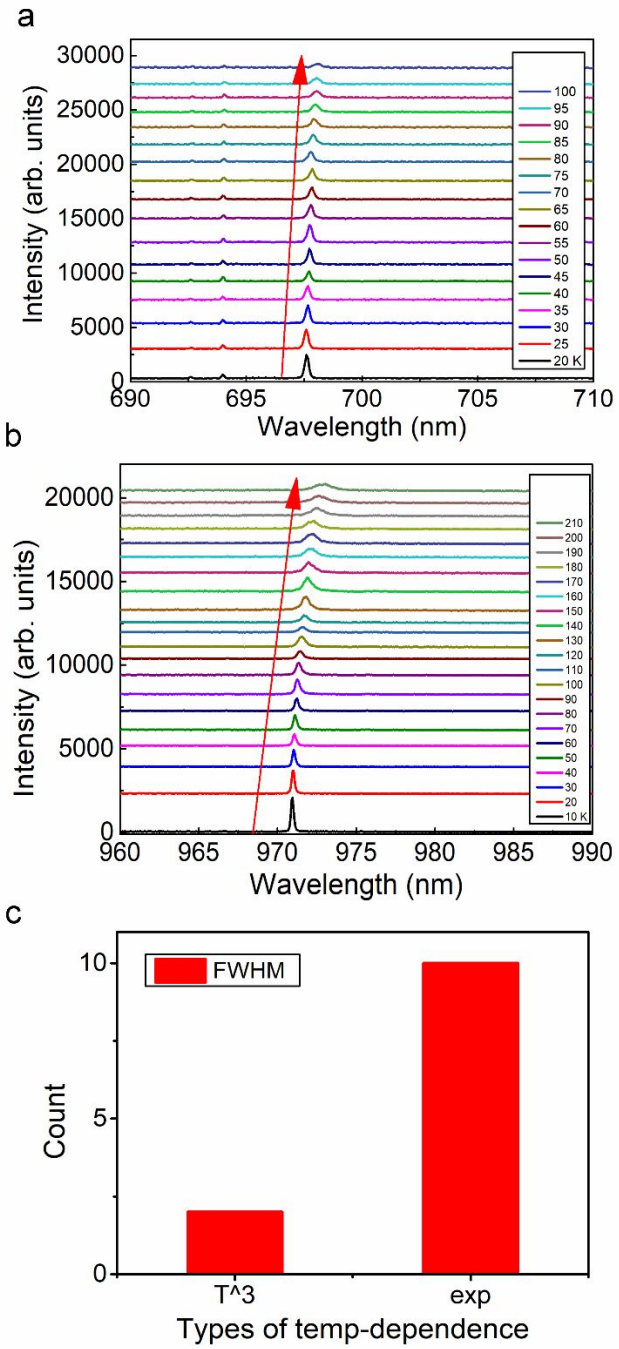

Figure S7. PL spectra measured under temperatures from 20 to 100 K (a) and from 10 to 210 K (b). (c) Histogram of temperature-dependent FWHMs for 12 different

emitters.

V. Density Functional Theory (DFT) calculations

We choose the supercell consisting of 3 × 3 × 2 AlN primitive cells (72 atoms) for the defect calculation. The bigger supercell containing 96 atoms is also tested. The results of dielectric function and the peak energy of the optical response are similar for different dimensions, which indicates our surpercell selection of defect calculations is reasonable.

Considering the GGA-PBE method usually underestimates the bandgap of materials, we corrected the bandgaps by using the GGA-1/2 method,[3] and the corresponding optical properties of defect AlN systems are also calculated. For $N_{Al}V_N$ defect system, the GGA-1/2 estimated peak energy of the optical response is 1.39 eV (892 nm), and in the case of $V_{Al}V_N$, an optical response around 2.17 eV (571 nm) exists. Compared with GGA-PBE results, there are some deviations in the GGA-1/2 estimated peaks. However, both of the estimated peak energies are in the observed emission range of 550-1000 nm, which further verifies the conclusion that the $N_{Al}V_N$ and $V_{Al}V_N$ defects are the most likely origin of the emission lines in our experiments.

For the vacancies shown in Fig. S8 (a) and (b), there are obvious emissions of peak energy around 0.52 and 0.97 eV in V_{Al} defect, and two optical transitions of 0.24 and 3.90 eV in V_N defect. An obvious emission peak of approximately 1.21 eV exits in the N_{Al} defect (Figure S8 (c)), which is close to the wavelength range for single-photon emissions in our experiments. Figures S8 (d) and (e) show that the corresponding energy peak of the O_N defect is 0.60 eV, while there is no obvious single emission

peak from C_N defect centers. For the complex defect $V_{Al}O_N$ in Fig. S8 (f), there are two obvious emission peaks at 0.47 and 0.75 eV. All of the above results are inconsistent with our experimental data.

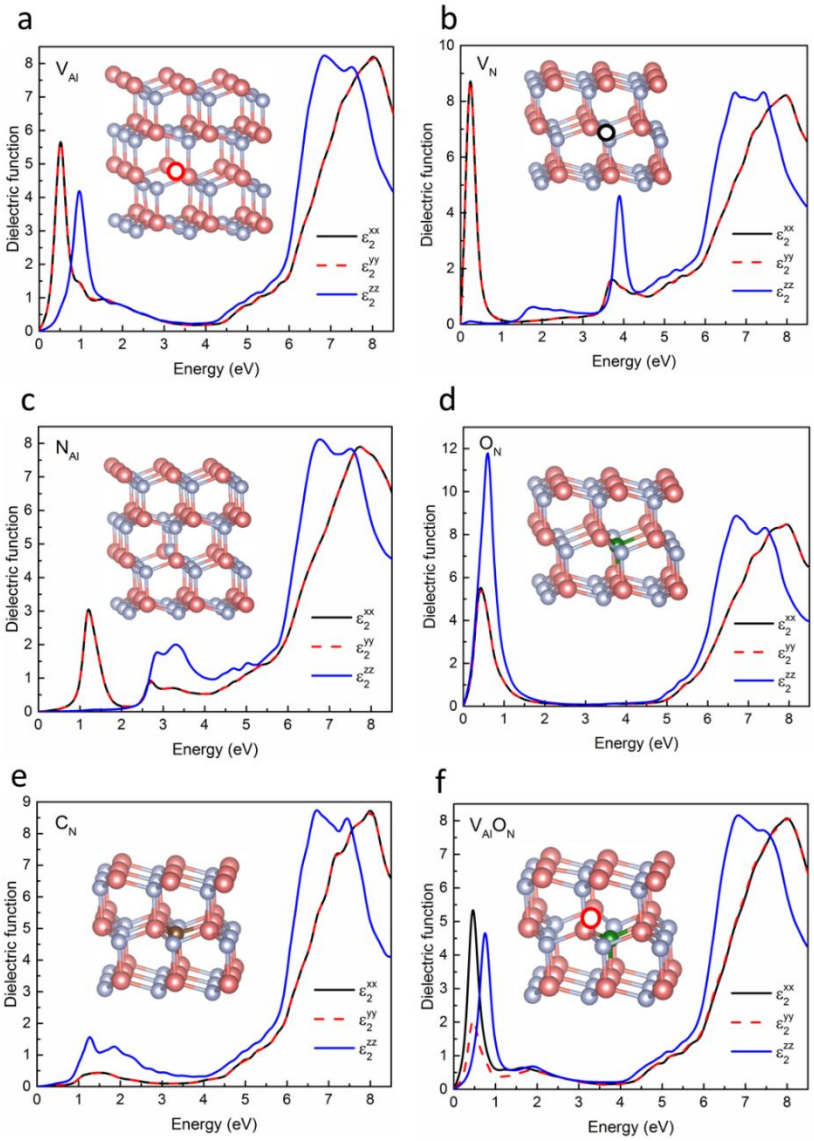

Figure S8. Calculated imaginary part of the dielectric function.

Reference

(1) Shen, L.; Wang, N.; Xiao, X. Strong Orange Luminescence from AlN Whiskers. *Mater. Lett.* **2013**, *94*, 150-153.

(2) Liu, G.; Yan, C.; Zhou, G.; Wen, J.; Qin, Z.; Zhou, Q.; Li, B.; Zheng, R.; Sun, Z. Broadband White-Light Emission from Alumina Nitride Bulk Single Crystals. *ACS*

Photonics **2018**, *5*, 4009-4013.

(3) Ferreira, L. G.; Marques, M.; Teles, L. K. Approximation to Density Functional Theory for the Calculation of Band Gaps of Semiconductors. *Phys. Rev. B* **2008**, *78*, 125116.